

Nodeless superconductivity in $\text{Ir}_{1-x}\text{Pt}_x\text{Te}_2$ with strong spin-orbital coupling

S. Y. Zhou,¹ B. Y. Pan,¹ X. Qiu,¹ J. Pan,¹ X. C. Hong,¹ X. L. Li,¹ Z. Zhang,¹ J. J. Yang,² Y. S. Oh,³ S-W. Cheong,^{2,3} and S. Y. Li^{1,*}

¹State Key Laboratory of Surface Physics, Department of Physics, and Laboratory of Advanced Materials, Fudan University, Shanghai 200433, P. R. China

²Laboratory for Pohang Emergent Materials and Department of Physics, Pohang University of Science and Technology, Pohang 790-784, Korea

³Rutgers Center for Emergent Materials and Department of Physics & Astronomy, Rutgers University, Piscataway, New Jersey 08854, USA

(Dated: April 27, 2019)

The thermal conductivity κ of the layered superconductor $\text{Ir}_{1-x}\text{Pt}_x\text{Te}_2$ with strong spin-orbital coupling was measured down to 50 mK. For optimally doped $\text{Ir}_{0.96}\text{Pt}_{0.04}\text{Te}_2$ polycrystal, a very small residual linear term κ_0/T , only about 1% of its normal-state value, is observed in zero field. In low magnetic field, κ_0/T shows a very slow field dependence. For inhomogeneous $\text{Ir}_{1-x}\text{Pt}_x\text{Te}_2$ single crystal with nominal $x = 0.2$, the κ_0/T in zero field is about 23% of its normal-state value, but the overall field dependence of κ_0/T is also slow. We attribute the finite κ_0/T in zero field to the nonsuperconducting impure phase in the samples, and the slow field dependence of κ_0/T manifests the underlying nodeless superconducting gap in $\text{Ir}_{1-x}\text{Pt}_x\text{Te}_2$, which puts strict constrain on the pairing symmetry.

PACS numbers: 74.25.fc, 74.40.Kb, 74.25.Op

I. INTRODUCTION

The effect of strong spin-orbital coupling (SOC) on superconductivity has recently attracted much attention. One example is the topological superconductor, such as candidate $\text{Cu}_x\text{Bi}_2\text{Se}_3$ in which Cu atoms are intercalated into topological insulator Bi_2Se_3 with strong SOC.¹ Novel superconducting state was claimed in $\text{Cu}_x\text{Bi}_2\text{Se}_3$ by the point-contact spectra and superfluid density measurements.^{2,3} Another example is the noncentrosymmetric superconductor, such as $\text{Li}_2\text{Pt}_3\text{B}$ in which the spatial inversion symmetry is broken.⁴ The strong SOC in $\text{Li}_2\text{Pt}_3\text{B}$ gives large spin-triplet pairing component and produces line nodes in the superconducting gap.^{5,6}

More recently, superconductivity was discovered in the layered compound IrTe_2 by Pd intercalation (Pd_xIrTe_2), Pd substitution ($\text{Ir}_{1-x}\text{Pd}_x\text{Te}_2$), or Pt substitution ($\text{Ir}_{1-x}\text{Pt}_x\text{Te}_2$).^{7,8} The parent compound IrTe_2 shows a charge-orbital density wave (DW) type transition at ~ 262 K.⁷ With increasing the doping level x , the DW transition is gradually suppressed and superconductivity emerges, showing a domelike phase diagram with the maximum T_c of 3 K near $x \approx 0.04$.^{7,8}

Since the SOC is proportional to Z^4 , where Z is the atomic number, the superconductivity in doped IrTe_2 must associated with strong SOC due to the large Z . Therefore it is of great interest to investigate whether there is novel superconducting state in doped IrTe_2 , as in $\text{Cu}_x\text{Bi}_2\text{Se}_3$.^{2,3} Furthermore, the phase diagram of doped IrTe_2 is reminiscent of high- T_c cuprates and some heavy fermion superconductors, in which superconductivity appears close to a magnetic quantum critical point (QCP). This means that there likely exists a QCP of charge-orbital DW under the superconducting dome of doped

IrTe_2 , and the DW fluctuations may give unconventional superconductivity.⁹

The ultra-low-temperature thermal conductivity measurement is a bulk tool to study the gap structure of superconductors.¹⁰ The existence of a finite residual linear term κ_0/T in zero field is usually considered as the signature of nodal superconducting gap. Further information of nodal gap, gap anisotropy, or multiple gaps may be obtained from the field dependence of κ_0/T .¹⁰ Previously, single-gap s -wave superconductivity near the QCP of charge DW has been clearly shown in Cu_xTiSe_2 by thermal conductivity measurements.¹¹

In this paper, we probe the superconducting gap structure of $\text{Ir}_{1-x}\text{Pt}_x\text{Te}_2$ by measuring the thermal conductivity κ down to 50 mK. Although a residual linear term κ_0/T is observed in zero field for both $\text{Ir}_{0.96}\text{Pt}_{0.04}\text{Te}_2$ polycrystal and nominal $\text{Ir}_{0.8}\text{Pt}_{0.2}\text{Te}_2$ single crystal, the field dependence of κ_0/T is rather slow at low field, unlike that of a nodal superconductor. We attribute the finite κ_0/T in zero field to the nonsuperconducting impure phase in the samples, while the overall slow field dependence of κ_0/T suggests nodeless superconducting gap in $\text{Ir}_{1-x}\text{Pt}_x\text{Te}_2$.

II. EXPERIMENTAL

Polycrystal of $\text{Ir}_{0.96}\text{Pt}_{0.04}\text{Te}_2$ was prepared as described in ref. 7. Single crystals of $\text{Ir}_{1-x}\text{Pt}_x\text{Te}_2$ superconductors were grown by the flux method for the first time.¹² It is found that the homogeneous $\text{Ir}_{1-x}\text{Pt}_x\text{Te}_2$ single crystals with large superconducting volume fraction are very difficult to obtain, which is similar to the case of $\text{Cu}_x\text{Bi}_2\text{Se}_3$.^{1,13} Despite of the inhomogeneity, we choose the best superconducting single crystal available,

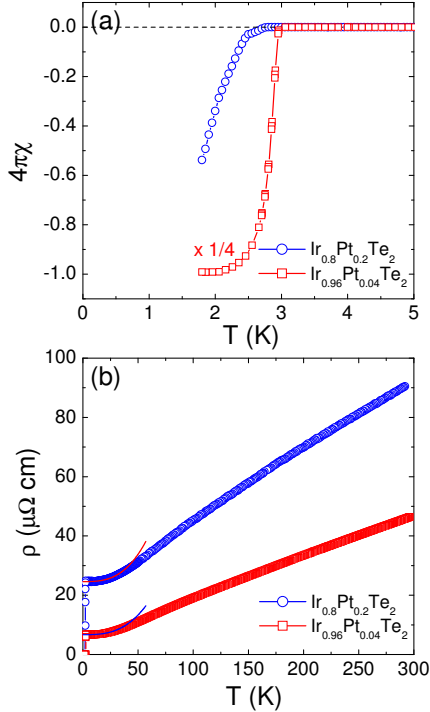


FIG. 1: (Color online). (a) Magnetic susceptibility of the $\text{Ir}_{0.96}\text{Pt}_{0.04}\text{Te}_2$ polycrystal and the $\text{Ir}_{1-x}\text{Pt}_x\text{Te}_2$ single crystal with nominal $x = 0.2$. (b) Resistivity of the $\text{Ir}_{0.96}\text{Pt}_{0.04}\text{Te}_2$ polycrystal and the nominal $\text{Ir}_{0.8}\text{Pt}_{0.2}\text{Te}_2$ single crystal. For $\text{Ir}_{0.96}\text{Pt}_{0.04}\text{Te}_2$ sample, the data between 3.5 and 30 K can be fitted to $\rho(T) = \rho_0 + AT^n$, with $\rho_0 = 6.69 \pm 0.01 \mu\Omega\text{cm}$ and $n = 2.90 \pm 0.03$. For $\text{Ir}_{0.8}\text{Pt}_{0.2}\text{Te}_2$ sample, the same fit to the data between 3 and 30 K gives $\rho_0 = 24.60 \pm 0.01 \mu\Omega\text{cm}$ and $n = 2.92 \pm 0.09$.

with the nominal composition $\text{Ir}_{0.8}\text{Pt}_{0.2}\text{Te}_2$.

The $\text{Ir}_{0.96}\text{Pt}_{0.04}\text{Te}_2$ polycrystal was polished to a rectangular shape of dimensions $2.5 \times 0.7 \times 0.06 \text{ mm}^3$. The $\text{Ir}_{0.8}\text{Pt}_{0.2}\text{Te}_2$ single crystal was cleaved to $2.0 \times 0.7 \text{ mm}^2$ in the ab plane, with $40 \mu\text{m}$ thickness along the c axis. The dc magnetic susceptibility was measured by using a SQUID (MPMS, Quantum Design). Four silver wires were attached to the sample with silver paint, which were used for both resistivity and thermal conductivity measurements. The contacts are metallic with typical resistance $10 \text{ m}\Omega$ at 2 K. Thermal conductivity was measured in a dilution refrigerator, using a standard four-wire steady-state method with two RuO_2 chip thermometers, calibrated *in situ* against a reference RuO_2 thermometer. Magnetic fields were applied perpendicular to the largest surface of the samples. To ensure a homogeneous field distribution in the samples, all fields were applied at temperature above T_c .

III. RESULTS AND DISCUSSION

Figure 1(a) presents the dc magnetic susceptibility of the $\text{Ir}_{0.96}\text{Pt}_{0.04}\text{Te}_2$ polycrystal and $\text{Ir}_{1-x}\text{Pt}_x\text{Te}_2$ single

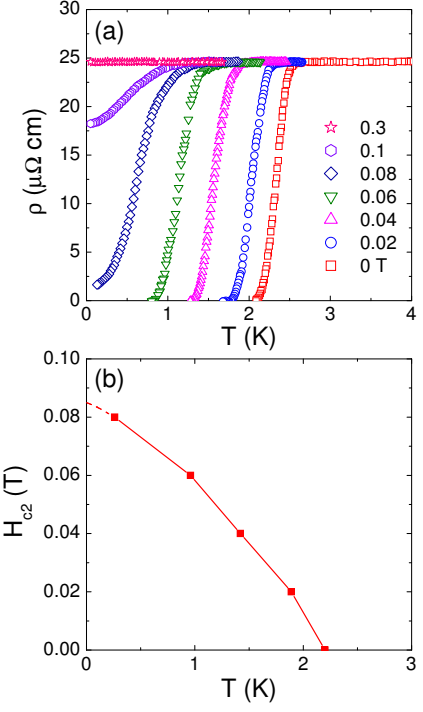


FIG. 2: (Color online). (a) Resistivity of the nominal $\text{Ir}_{0.8}\text{Pt}_{0.2}\text{Te}_2$ single crystal (OD20) in magnetic field up to 0.3 T. (b) Temperature dependence of the upper critical field $H_{c2}(T)$, defined at the point dropping to 10% of the normal-state resistivity on the curves in (a). The dashed line is a guide to the eye, which points to $H_{c2}(0) \approx 0.085 \text{ T}$.

crystal with nominal $x = 0.2$. It was measured in $H = 20 \text{ Oe}$ perpendicular to the largest surface, with zero field cooled. The $\text{Ir}_{0.96}\text{Pt}_{0.04}\text{Te}_2$ polycrystal shows a very sharp superconducting transition with $T_c \approx 3.0 \text{ K}$ and very large superconducting volume fraction, suggesting that it is a homogeneous bulk superconductor at optimal doping. For the nominal $\text{Ir}_{0.8}\text{Pt}_{0.2}\text{Te}_2$ single crystal, the onset of diamagnetic transition is at 2.7 K, and the transition does not complete down to 1.8 K. Since the T_c of this sample is lower than the optimal $T_c \approx 3 \text{ K}$, it should be on the overdoped side. The superconducting volume fraction is about 55% at 1.8 K, showing bulk superconductivity of the sample. However, the wide transition indicates inhomogeneity of Pt content inside the sample. Hereafter these two samples are named OP04 and OD20.

Figure 1(b) shows the resistivity of OP04 and OD20 in zero field. No resistivity anomaly is observed above T_c , which suggests that no DW transition occurs in our samples. This confirms OD20 is on the overdoped side. For OP04, the data between 3.5 and 30 K can be fitted to $\rho(T) = \rho_0 + AT^n$, with $\rho_0 = 6.69 \pm 0.01 \mu\Omega\text{cm}$ and $n = 2.90 \pm 0.03$. For OD20, the same fit to the data between 3 and 30 K gives $\rho_0 = 24.60 \pm 0.01 \mu\Omega\text{cm}$ and $n = 2.92 \pm 0.09$. Such a temperature dependence of $\rho(T)$ has been observed in $\text{Ir}_{1-x}\text{Pt}_x\text{Te}_2$ polycrystal and attributed to phonon-assisted interband scattering,⁸ as in TiSe_2 .¹⁴

Previously, the upper critical field $H_{c2}(0) \approx 0.17 \text{ T}$

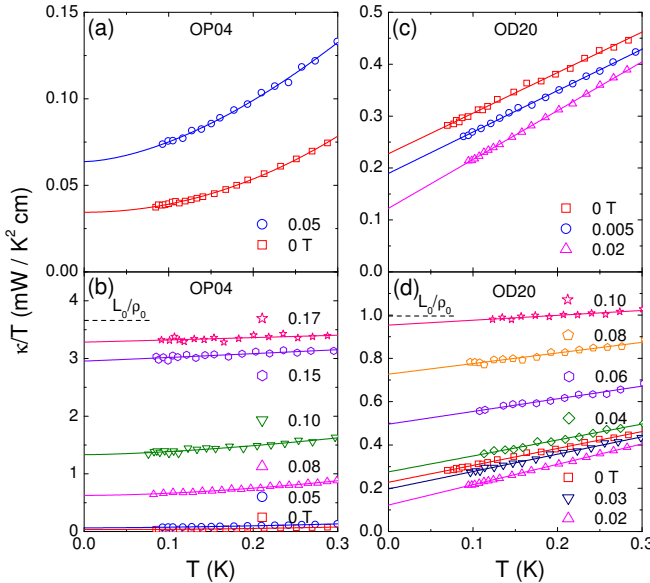


FIG. 3: (Color online). Low-temperature thermal conductivity of the $\text{Ir}_{0.96}\text{Pt}_{0.04}\text{Te}_2$ polycrystal (OP04) and the nominal $\text{Ir}_{0.8}\text{Pt}_{0.2}\text{Te}_2$ single crystal (OD20) in zero and magnetic fields. The solid lines are fits to $\kappa/T = a + bT^{\alpha-1}$. For OD20, α is fixed to 2. The dash lines are the normal-state Wiedemann-Franz law expectation L_0/ρ_0 , with L_0 the Lorenz number $2.45 \times 10^{-8} \text{ W}\Omega\text{K}^{-2}$, $\rho_0 = 6.69$ and $24.60 \mu\Omega\text{cm}$, respectively.

has been determined for $\text{Ir}_{0.96}\text{Pt}_{0.04}\text{Te}_2$ polycrystal by resistivity measurement.⁸ In order to obtain the $H_{c2}(0)$ of OD20, we also measure its resistivity in field up to $H = 0.3$ T and down to 50 mK, shown in Fig. 2(a). The superconducting transition is gradually suppressed and no transition is observed down to 50 mK in $H = 0.3$ T. In Fig. 2(b), we plot the temperature dependence of H_{c2} , defined at the point dropping to 10% of the normal-state resistivity on the curves in Fig. 2(a). The dashed line is a guide to the eye, which points to $H_{c2}(0) \approx 0.085$ T.

The thermal conductivity of OP04 in zero and finite magnetic fields are plotted in Fig. 3(a) and 3(b), as κ/T vs T . We fit all the curves to $\kappa/T = a + bT^{\alpha-1}$, in which the two terms aT and bT^α represent contributions from electrons and phonons, respectively.^{15,16} The power α of the second term contributed by phonons is typically between 2 and 3 for single crystals, due to specular reflections of phonons at the boundary.^{15,16} For OP04 polycrystal in zero field, the fitting gives a residual linear term $\kappa_0/T = 34.4 \pm 0.5 \mu\text{W K}^{-2} \text{ cm}^{-1}$, with $\alpha = 3.03 \pm 0.07$. This value of κ_0/T is not negligible comparing to our experimental error bar $5 \mu\text{W K}^{-2} \text{ cm}^{-1}$, however it is only about 1% of the normal-state Wiedemann-Franz law expectation $\kappa_{N0}/T = L_0/\rho_0 = 3.66 \text{ mW K}^{-2} \text{ cm}^{-1}$, with L_0 the Lorenz number $2.45 \times 10^{-8} \text{ W}\Omega\text{K}^{-2}$ and normal-state $\rho_0 = 6.69 \mu\Omega\text{cm}$.

In Fig. 3(c) and 3(d), the in-plane thermal conductivity of OD20 in magnetic field up to $H = 0.10$ T are also plotted as κ/T vs T . All the curves are

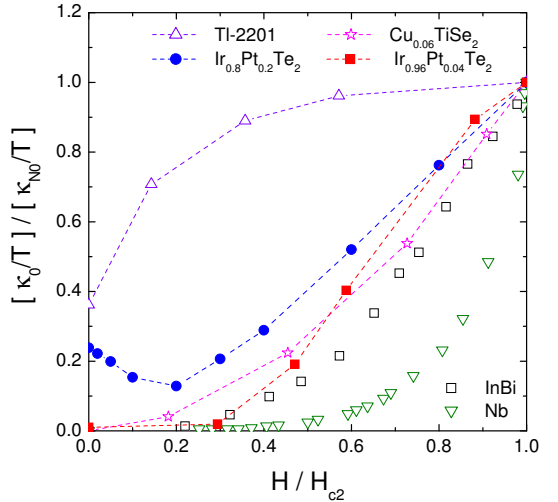


FIG. 4: (Color online). Normalized residual linear term κ_0/T of the $\text{Ir}_{0.96}\text{Pt}_{0.04}\text{Te}_2$ polycrystal (OP04) and the nominal $\text{Ir}_{0.8}\text{Pt}_{0.2}\text{Te}_2$ single crystal (OD20) as a function of H/H_{c2} . For comparison, similar data are shown for the clean s -wave superconductor Nb,²⁴ the dirty s -wave superconducting alloy InBi,²⁵ an overdoped d -wave cuprate superconductor Tl-2201,²⁰ and the single-gap s -wave superconductor $\text{Cu}_{0.06}\text{TiSe}_2$.¹¹

roughly linear. Therefore we fit all the curves to $\kappa/T = a + bT^{\alpha-1}$ with α fixed to 2. Previously $\alpha \approx 2.2$ was found in $\text{Cu}_{0.06}\text{TiSe}_2$,¹¹ and recently $\alpha \approx 2$ has been observed in some iron-based superconductors such as $\text{BaFe}_{1.9}\text{Ni}_{0.1}\text{As}_2$,¹⁷ KFe_2As_2 ,¹⁸ and $\text{Ba}(\text{Fe}_{1-x}\text{Ru}_x)_2\text{As}_2$ single crystals.¹⁹ For OD20 in zero field, the fitting gives a residual linear term $\kappa_0/T = 0.228 \pm 0.002 \text{ mW K}^{-2} \text{ cm}^{-1}$. This value is about 23% of the normal-state Wiedemann-Franz law expectation $\kappa_{N0}/T = L_0/\rho_0 = 1.00 \text{ mW K}^{-2} \text{ cm}^{-1}$, with $\rho_0 = 24.60 \mu\Omega\text{cm}$.

Usually, a finite κ_0/T in zero field comes from the nodal quasiparticles in a superconductor with nodal gap.¹⁰ For example, $\kappa_0/T = 1.41 \text{ mW K}^{-2} \text{ cm}^{-1}$ for the overdoped cuprate $\text{Tl}_2\text{Ba}_2\text{CuO}_{6+\delta}$ (Tl-2201), a d -wave superconductor with $T_c = 15$ K,²⁰ and $\kappa_0/T = 17 \text{ mW K}^{-2} \text{ cm}^{-1}$ for the ruthenate Sr_2RuO_4 , a p -wave superconductor with $T_c = 1.5$ K.²¹ However, if some nonsuperconducting but metallic impure phase exists in a nodeless superconductor, it will also contribute a finite κ_0/T in zero field. For example, $\kappa_0/T = 0.3 \text{ mW K}^{-2} \text{ cm}^{-1}$, $\sim 7\%$ of the normal-state value, was observed and attributed to the inclusions of pure graphite in the single-gap s -wave superconductor C_6Yb with $T_c = 5.4$ K.²²

Since a very small amount of impure phase in the OP04 polycrystal is possible and the OD20 single crystal is inhomogeneous, it is essential to check their field dependence of κ_0/T to distinguish between above two cases. In the case of nodal superconductor, κ_0/T increases rapidly ($\sim H^{1/2}$) in low field due to the Volovik effect,²³ as in Tl-2201.²⁰ However, in the case of single-gap s -wave superconductor containing nonsuperconducting but metallic impure phase, κ_0/T displays a slow field dependence

at low field, as in C_6Yb .²² In Fig. 3, all the data of OP04 and OD20 are fitted and κ_0/T is obtained for each magnetic field. Note that in the field of $H = 0.17$ T for OP04 and 0.10 T for OD20, the Wiedemann-Franz law is roughly satisfied for both samples, respectively, which gives their bulk $H_{c2}(0)$. A slightly different $H_{c2}(0)$ does not affect our discussion on the field dependence of κ_0/T below.

In Fig. 4, the normalized κ_0/T of OP04 and OD20 are plotted as a function of H/H_{c2} . For comparison, we also plot the data of the clean s -wave superconductor Nb,²⁴ the dirty s -wave superconducting alloy InBi,²⁵ the d -wave cuprate superconductor Tl-2201,²⁰ and the s -wave superconductor $Cu_{0.06}TiSe_2$.¹¹ From Fig. 4, the κ_0/T of OP04 shows a very slow field dependence at low field, which is similar to that of s -wave superconductors $Cu_{0.06}TiSe_2$ and InBi. This suggests the second case for OP04, i.e., a nodeless superconductor with a very small amount of nonsuperconducting but metallic impure phase.

For OD20 sample, κ_0/T decreases at low field first, then it increases slowly above $H \approx 0.02$ T. Since our OD20 sample is inhomogenous and on the overdoped side ($x > 0.04$), we attribute the finite κ_0/T of OD20 in zero field to nonsuperconducting but metallic phase with $x > 0.10$, and the overall slow field dependence of κ_0/T manifests the underlying nodeless superconducting gap, as in C_6Yb .²² By assuming the same ρ_0 for different doping level in our sample, some 23% volume fraction of nonsuperconducting impure phase will give the κ_0/T in zero field. Since the magnetoresistance of our sample is negligible, the decrease of κ_0/T in low field should not come from the magnetoresistance effect of the nonsuperconducting impure phase. Actually, it may be explained by vortex scattering. Above the lower critical field H_{c1} , the vortex will enter into the sample, which will scatter those normal electrons contributed by the nonsuperconducting impure phase, and reduce the κ_0/T .

Nodeless gap does not essentially mean conventional superconductivity. For example, the nodeless gap observed in optimally doped iron-based superconductor may be unconventional s_{\pm} -wave resulting from antiferromagnetic spin fluctuations.²⁶ However, here in $Ir_{1-x}Pt_xTe_2$, the nodeless gap is unlikely s_{\pm} -wave, despite that there may exist charge-orbital DW fluctuations.⁷ One obvious reason is that $Ir_{1-x}Pt_xTe_2$ does not have that kind of multiple Fermi surfaces as iron-based superconductors.^{7,26} Since previously nodeless

superconductivity has been observed in Cu_xTiSe_2 associated with a QCP of charge DW, it may not come as a surprise that we observe nodeless superconductivity again in $Ir_{1-x}Pt_xTe_2$ with a QCP of charge-orbital DW. In both systems, the appearance of superconductivity may have little to do with the DW fluctuations.

From the aspect of strong SOC, an unconventional odd-parity pairing state was claimed for the topological superconductor candidate $Cu_xBi_2Se_3$.^{2,3} However, both nodeless gap or gap with point nodes are allowed for the odd-parity superconducting state.² In this context, our finding of nodeless superconductivity in $Ir_{1-x}Pt_xTe_2$ with strong SOC does not completely exclude novel superconducting state. More experiments are needed to clarify this issue.

IV. SUMMARY

In summary, we investigate the superconducting gap structure of optimally doped $Ir_{0.96}Pt_{0.04}Te_2$ polycrystal and overdoped nominal $Ir_{0.8}Pt_{0.2}Te_2$ single crystal by thermal conductivity measurements. The overall slow field dependence of κ_0/T at low field supports nodeless superconductivity, while the finite κ_0/T in zero field is attributed to the nonsuperconducting but metallic impure phase in the samples. Our result puts a strict constraint on the paring symmetry of this system, when one considers the effect of strong spin-orbital coupling and density-wave fluctuations on the superconductivity.

ACKNOWLEDGEMENTS

This work is supported by the Natural Science Foundation of China, the Ministry of Science and Technology of China (National Basic Research Program No: 2009CB929203 and 2012CB821402), and the Program for Professor of Special Appointment (Eastern Scholar) at Shanghai Institutions of Higher Learning. The research at Postech and Rutgers University was supported by the Max Planck POSTECH/KOREA Research Initiative Program [Grant No. 2011-0031558] through NRF of Korea funded by MEST and the NSF under Grant No. NSFDMR-1104484, respectively.

* E-mail: shiyan_li@fudan.edu.cn

¹ Y. S. Hor, A. J. Williams, J. G. Checkelsky, P. Roushan, J. Seo, Q. Xu, H.W. Zandbergen, A. Yazdani, N. P. Ong, and R. J. Cava, Phys. Rev. Lett. **104**, 057001 (2010).

² S. Sasaki, M. Kriener, K. Segawa, K. Yada, Y. Tanaka, M. Sato, and Y. Ando, Phys. Rev. Lett. **107**, 217001 (2011).

³ M. Kriener, Kouji Segawa, Satoshi Sasaki, and Yoichi Ando, arXiv:1206.6260.

⁴ P. Badica, T. Kondo, and K. Togano, J. Phys. Soc. Jpn.

74, 1014 (2005).

⁵ H. Q. Yuan, D. F. Agterberg, N. Hayashi, P. Badica, D. Vandervelde, K. Togano, M. Sigrist, and M. B. Salamon, Phys. Rev. Lett. **97**, 017006 (2006).

⁶ M. Nishiyama, Y. Inada, and Guo-qing Zheng, Phys. Rev. Lett. **98**, 047002 (2007).

⁷ J. J. Yang, Y. J. Choi, Y. S. Oh, A. Hogan, Y. Horibe, K. Kim, B. I. Min, and S-W. Cheong, Phys. Rev. Lett. **108**,

⁸ 116402 (2012).

⁸ S. Pyon, K. Kudo, and M. Nohara, *J. Phys. Soc. Jpn.* **81**, 053701 (2012).

⁹ P. Monthoux and G. G. Lonzarich, *Phys. Rev. B* **69**, 064517 (2004).

¹⁰ H. Shakeripour, C. Petrovic and L. Taillefer, *New J. Phys.* **11**, 055065 (2009).

¹¹ S. Y. Li, G. Wu, X. H. Chen, and Louis Taillefer, *Phys. Rev. Lett.* **99**, 107001 (2007).

¹² J. J. Yang, Y. S. Oh, and S-W. Cheong, unpublished.

¹³ M. Kriener, K. Segawa, Z. Ren, S. Sasaki, S. Wada, S. Kuwabata, and Y. Ando, *Phys. Rev. B* **84**, 054513 (2011).

¹⁴ A. F. Kusmartseva, B. Sipos, H. Berger, L. Forró, and E. Tutuš, *Phys. Rev. Lett.* **103**, 236401 (2009).

¹⁵ M. Sutherland, D. G. Hawthorn, R. W. Hill, F. Ronning, S. Wakimoto, H. Zhang, C. Proust, E. Boaknin, C. Lupien, Louis Taillefer, Ruixing Liang, D. A. Bonn, W. N. Hardy, Robert Gagnon, N. E. Hussey, T. Kimura, M. Nohara, and H. Takagi, *Phys. Rev. B* **67**, 174520 (2003).

¹⁶ S. Y. Li, J.-B. Bonnemaison, A. Payeur, P. Fournier, C. H. Wang, X. H. Chen, and L. Taillefer, *Phys. Rev. B* **77**, 134501 (2008).

¹⁷ L. Ding, J. K. Dong, S. Y. Zhou, T. Y. Guan, X. Qiu, C. Zhang, L. J. Li, X. Lin, G. H. Cao, Z. A. Xu and S. Y. Li, *New J. Phys.* **11**, 093018 (2009).

¹⁸ J. K. Dong, S. Y. Zhou, T. Y. Guan, H. Zhang, Y. F. Dai, X. Qiu, X. F. Wang, Y. He, X. H. Chen, and S. Y. Li, *Phys. Rev. Lett.* **104**, 087005 (2010).

¹⁹ X. Qiu, S. Y. Zhou, H. Zhang, B. Y. Pan, X. C. Hong, Y. F. Dai, Man Jin Eom, Jun Sung Kim, Z. R. Ye, Y. Zhang, D. L. Feng, and S. Y. Li, *Phys. Rev. X* **2**, 011010 (2012).

²⁰ C. Proust, E. Boaknin, R. W. Hill, Louis Taillefer, and A. P. Mackenzie, *Phys. Rev. Lett.* **89**, 147003 (2002).

²¹ M. Suzuki, M. A. Tanatar, N. Kikugawa, Z. Q. Mao, Y. Maeno, and T. Ishiguro, *Phys. Rev. Lett.* **88**, 227004 (2002).

²² M. Sutherland, N. Doiron-Leyraud, Louis Taillefer, T. Weller, M. Ellerby, and S. S. Saxena, *Phys. Rev. Lett.* **98**, 067003 (2007).

²³ G. E. Volovik, *JETP Lett.* **58**, 469 (1993).

²⁴ J. Lowell and J. Sousa, *J. Low. Temp. Phys.* **3**, 65 (1970).

²⁵ J. Willis and D. Ginsberg, *Phys. Rev. B* **14**, 1916 (1976).

²⁶ P. J. Hirschfeld, M. M. Korshunov, and I. I. Mazin, *Rep. Prog. Phys.* **74**, 124508 (2011).